Molecular conformations of dumbbell-shaped polymers in good solvent

Khristine Haydukivska,[1,2] V. Blavatska,[2,3] and Jarosław Paturej[1,4,*]

[1]*Institute of Physics, University of Silesia, 41-500 Chorzów, Poland*

[2]*Institute for Condensed Matter Physics of the National Academy of Sciences of Ukraine, 79011 Lviv, Ukraine*

[3]*Dioscuri Centre for Physics and Chemistry of Bacteria, Institute of Physical Chemistry, Polish Academy of Sciences, 01-224 Warsaw, Poland*

[4]*Leibniz-Institut für Polymerforschung Dresden e.V., 01069 Dresden, Germany*

(Received 21 March 2023; accepted 11 August 2023; published 5 September 2023)

We study conformational properties of diluted dumbbell polymers composed of two rings attached to both ends of a linear spacer segment. Our investigation involves analytical methods of field theory and bead-spring coarse-grained molecular dynamics simulations. We focus on the influence of the relative length of the spacer segment to the length of side rings on the shape and the relative size of dumbbells as compared to linear polymers of equal mass. We find that dumbbells with short spacers exhibit a significantly more compact structure than linear polymers. Conversely, as the spacer length increases, the influence of the side rings on the size of the dumbbells becomes negligible. Consequently, dumbbell molecules with long spacers attain a size comparable to corresponding linear chains. Our analytical theory accurately predicts a quantitative conformational crossover between the behaviors of short-spacer and long-spacer dumbbells, which is further confirmed by our numerical simulations.

DOI: 10.1103/PhysRevE.108.034502

I. INTRODUCTION

In recent decades a lot of attention has been directed to the research of polymers that go beyond standard linear molecular architectures. Particularly interesting are ring polymers with no free ends [1–3]. Ring polymers are observed in nature in bacteria [4] and in some higher eukaryotes [5] which contain a circular DNA. Ring polymers exhibit unique physical and chemical properties that can make them advantageous with respect to their linear counterparts. This includes increased solubility, greater stability, and improved catalytic activity. For example, cyclic peptides and cyclic oligonucleotides are often used in drug discovery and development because their cyclic structure can increase their bioavailability and improve their ability to interact with target molecules. One of the main advantages of ring polymers with respect to their linear counterparts is their compact size which prevents the rings from becoming entangled and makes them the simplest model system where reptation is completely suppressed. Ring polymers have smaller size and hydrodynamic radius in solutions, lower melt viscosity due to lack of plateau modulus, much larger swelling factor and larger maximum strain at break in swollen networks, and higher thermostability [6–15]. The cyclic architecture lowers interpenetration and frictional forces between polymer coated surfaces [16] and allows one to tune domain spacing of self-assembled polymer materials [17].

Blending of rings with linear polymers as well as incorporation of cyclic grafts into linear architecture open new possibilities to control physical properties of polymeric materials. The viscosity of a linear-ring blend increases with increasing concentration of linear contaminants and for equal concentrations of linear and ring polymers is about twice that of the pure linear melt [18]. Covalent bonding of a ring to one end of a linear chain provides hybrid polymer architecture called a tadpole polymer which allows for further modification of viscoelastic properties. Melts of tad-pole polymers with linear tails above entanglement length exhibit a plateau modulus which is comparable to melts of linear polymers but have much slower terminal relaxation than their component ring and linear chains as well as slower than the ring/linear blends [19,20]. These properties are attributed to threading which is spontaneous intermolecular ring-linear penetration [21].

Dumbbell polymers consist of two rings that are attached to both ends of a linear chain segment. Recently dumbbell-shaped polymers (see Fig. 1) were investigated experimentally in dilute and concentrated solutions [22]. The viscosity of diluted dumbbell solution is comparable with that of pure linear chains. This suggests that the dumbbell molecules behave like an isolated linear chain in the dilute regime. Bulk dumbbells display an extremely long entanglement plateau, whereas their terminal relaxation behavior is not observed. The authors suggested that this specific behavior is due to formation of dynamic networks where two rings on both ends of a dumbbell molecule spontaneously thread with other dumbbells. This characteristic entanglement due to the intermolecular threading dominates typical entanglements observed in pure linear chain melts. On the other hand those same molecules in dilute solution have a similar behavior to that of the simple chains, in particular the similar values of viscosity where observed.

In this paper we investigate conformational properties of diluted dumbbell-shaped macromolecules in a good solvent. We characterize universal structural properties of these

*jaroslaw.paturej@us.edu.pl

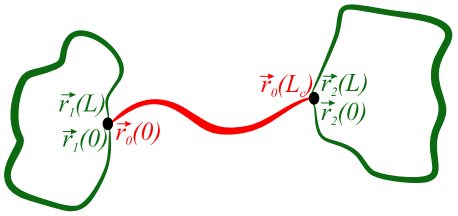

FIG. 1. Schematic representation of a dumbbell-shaped polymer composed of a linear spacer (red line) with two side rings (green lines) grafted to its ends.

polymers that depend only on global properties of the system such as the quality of solvent, polymer connectivity, and the space dimension, but do not depend on the details of the monomer chemistry. We analyze the degree of compactness of dumbbells with respect to the linear chains of the same molecular weight. The quantitative description of the relative size is calculated through the size ratio [6]

$$g_c = \frac{\langle R_g^2 \rangle}{\langle R_g^2 \rangle_{\text{linear}}}. \tag{1}$$

We also analyze the shape of dumbbell conformations using asphericity parameter $\langle A_d \rangle$ [23]. The quantity A_d measures the degree to which a molecule deviates from a perfect sphere. For spherical conformations it is $\langle A_d \rangle = 0$ whereas for rodlike configurations it is $\langle A_d \rangle = 1$. The asphericity is defined as

$$\langle A_d \rangle = \frac{1}{d(d-1)} \left\langle \frac{\text{Tr}\hat{\mathbf{S}}^2}{(\text{Tr}\mathbf{S})^2} \right\rangle \tag{2}$$

where $\mathbf{S}$ in the gyration tensor and $\hat{\mathbf{S}} = \mathbf{S} - \overline{\mu}\mathbf{I}$ with $\overline{\mu}$ being an average eigenvalue and $\mathbf{I}$ a unity matrix. We estimate g_c using an analytical theory based on the path-integration method. The parameter A_d is calculated using the graph theory approach developed by Wei [24]. The outcomes of our analytical calculations are compared with numerical data obtained from extensive bead-spring coarse-grained molecular dynamics (MD) modeling.

The paper is organized as follows. In Sec. II we start with description of theoretical and simulation methods utilized in this paper. The discussion of the results is presented in Sec. III. We conclude our findings in Sec. IV.

II. MODELS AND METHODS

A. Analytical model

An analytical description is conducted using the field-theoretical continuous chain model [25]. In this model the polymer chain is represented by a trajectory of length L parametrized by the radius vector $\vec{r}(s)$ where s varies from zero to L. The Hamiltonian of the model is given as

$$H = \frac{1}{2}\sum_{i=0}^{F-1}\int_0^{L_i} ds \left(\frac{d\vec{r}_i(s)}{ds}\right)^2 + \frac{u}{2}\sum_{i,j=0}^{F-1}\int_0^{L_i} ds' \times \int_0^{L_j} ds''\, \delta[\vec{r}_i(s') - \vec{r}_j(s'')]. \tag{3}$$

In the above equation F denotes functionality, i.e., a number of trajectories in the branched polymer architecture (for a dumbbell polymer it is $F = 3$), and u is a coupling constant that describes the strength of the excluded volume interactions. The polymer topology is introduced in the partition function of the system by fixing the end(s) of trajectories:

$$Z^{\text{DB}}_{L_c,L} = \frac{1}{Z_0^{\text{DB}}} \int D\vec{r}(s) \times \delta[\vec{r}_1(0) - \vec{r}_0(0)]\delta[\vec{r}_2(0) - \vec{r}_0(L_c)] \times \delta[\vec{r}_1(0) - \vec{r}_1(L)]\delta[\vec{r}_2(0) - \vec{r}_2(L)]\, e^{-H}, \tag{4}$$

where $\delta(\vec{r}_1(0) - \vec{r}_0(0))$ and $\delta(\vec{r}_2(0) - \vec{r}_0(L_c))$ describe the connectivity of ring trajectories parametrized by vectors $\vec{r}_1$ and $\vec{r}_2$ to the ends of the linear trajectory $\vec{r}_0$ and the remaining two δ functions impose geometrical constraints to which trajectories are subjected to form closed rings (see Fig. 1) and Z_0^{DB} is a partition function of the Gaussian chain. Note that in our paper we consider dumbbell topologies with trajectories of different length. The linear backbone trajectory has the length L_c whereas the trajectory of side rings has the length L. We also point out that since both L and L_c in our analytical model are considered to be infinitely long the difference in length is introduced by considering the ratio $\lim_{L,L_c\to\infty} L_c/L = l$. We also note that in the continuous chain model the averaging over possible configurations that is performed in the partition function includes all types of knot conformations of the rings. Typically, the locations of knots along the polymer chain are not restricted to some specific parts of chain conformation and are influenced, for example, by thermal fluctuations and interactions within the chain [26]. It is anticipated that the distribution of knot sizes will exhibit universality [27]. However, the presence of knots in polymer conformations is not distinguishable in our model. Though the knots can influence dynamic polymer properties such as rheological response [28], in the limit of infinitely long polymer chains knots do not influence the universal conformational characteristics (such as scaling exponents and critical amplitudes) [29–31].

In the continuous chain model the contribution from the excluded volume interactions is considered to be much smaller as compared to the Gaussian elasticity term. As a consequence all the observables are calculated as a perturbation series over the coupling constant u_0 [32]. In general the partition function has the following form:

$$Z(L, L_c) = Z_0[1 - u_0 Z_1(l, d) + \cdots] \tag{5}$$

where $u_0 = u(2\pi)^{-\frac{d}{2}} L^{2-\frac{d}{2}}$ is a dimensionless coupling constant. In the the case of a dumbbell polymer $Z_0 = (2\pi L)^{-d}$. The second coefficient $Z_1(l, d)$ in the above equation represents the contribution from the excluded volume interactions and is calculated using the diagrammatic technique. The final expression for the coefficient $Z_1(l, d)$ as well as the details of calculations are provided in the Appendix [see Eq. (A5)]. All the observables can be written in the form of Eq. (5). In particular the radius of gyration is given as

$$\langle R_g^2 \rangle = \langle R_g^2 \rangle_0 [1 - u_0 R_1(l, d) + \cdots] \tag{6}$$

where $\langle R_g^2 \rangle_0$ denotes the contribution from the Gaussian conformation and the term R_1 is the first-order approximation of steric interactions. The explicit formula for term R_1 is

provided in Eq. (22) and the sketch of calculation of this term is given in the Appendix.

In the continuous chain model all observables depend on the coupling constant u_0 that diverges as $L \to \infty$. In order to calculate finite physical value of the observable a renormalization has to be introduced such that $u_0^* \to u_R^*$ as $L \to \infty$. The direct polymer renormalization approach for the model given by the Hamiltonian [see Eq. (3)] leads to the following fixed points [32]:

$$\text{Gaussian}: u_R^* = 0 \qquad \text{at} \qquad d \geqslant 4, \tag{7}$$

$$\text{EV}: u_R^* = \frac{\epsilon}{8} \qquad \text{at} \qquad d < 4, \tag{8}$$

where $\epsilon = 4 - d$ denotes the deviation from the upper critical dimension. A final result in this approach is usually given as a series in ϵ and and an accurate quantitative result that can be compared with experimental data requires at the very least terms up to $\sim\epsilon^2$. However, this is hard to achieve for a case of complex branched polymers. To overcome this problem we will use the method proposed by Douglas and Freed [7]. It starts by considering a generalized scaling form for the radius of gyration:

$$\langle R_g^2 \rangle = \langle R_g^2 \rangle_0 \left(\frac{2\pi N}{\Lambda} \right)^{2\nu(\eta)-1} f_p(\eta), \tag{9}$$

where N is the degree of polymerization, Λ is the coarse-graining length scale [33], and $f_p(\eta)$ is a function that controls the solvent quality with η being the crossover variable. It is equal to 1 for $\eta = 0$ (Gaussian chain) and $1 + a$ for $\eta \to \infty$ which corresponds to the case of good solvent where a is a topology-dependent parameter. At this point it is important to note that $(\frac{2\pi N}{\Lambda})^{2\nu(\eta)-1}$ is the same for all molecular topologies and yields that the size ratio has the following general form:

$$g_x = \frac{\langle R_{g,1}^2 \rangle_0}{\langle R_{g,2}^2 \rangle_0} \frac{1 + a_1}{1 + a_2}. \tag{10}$$

This expression does not contain any approximations since the parameters a_1 and a_2 are functions of ϵ. The approximation itself comes into play when the connection between a renormalization group approach and that of the two-parameter model for a $d = 3$-dimensional space is made by the expression

$$a = \frac{3}{4}\frac{\epsilon}{8} R_1(l, d = 3) - \frac{1}{4} \tag{11}$$

where $R_1(l, d = 3)$ is the coefficient mentioned above but calculated for $d = 3$ which corresponds to two-parameter model calculation.

B. Molecular dynamics simulations

We consider a three-dimensional, bead-spring coarse-grained model [34] of a dumbbell polymer which is composed of N spherical beads in each of two rings and N_c beads in the linear backbone. Each bead has the size σ_{LJ} and equal mass m. The nonbonded interactions between monomers are taken into account by means of the Weeks-Chandler-Anderson (WCA) interaction, i.e., the shifted and truncated repulsive branch of the Lennard-Jones (LJ) potential given by

$$V^{\text{WCA}}(r) = 4\epsilon_{\text{LJ}}[(\sigma_{\text{LJ}}/r)^{12} - (\sigma_{\text{LJ}}/r)^6 + 1/4]\theta(2^{1/6}\sigma_{\text{LJ}} - r). \tag{12}$$

In the above equation r denotes the distance between the centers of spherical beads, while ϵ and σ_{LJ} are chosen as units of energy and length, respectively. In Eq. (12) is the Heaviside step function $\theta(x) = 0$ or 1 for $x < 0$ or $x \geqslant 0$. The bonds between subsequent beads are described by the Kremer-Grest potential [35] $V^{\text{KG}}(r) = V^{\text{FENE}}(r) + V^{\text{WCA}}(r)$, where the first term represents by the finitely extensible nonlinear elastic (FENE) spring modeled by the following potential:

$$V^{\text{FENE}}(r) = -0.5kr_0^2 \ln[1 - (r/r_0)^2]. \tag{13}$$

with two constants $k = 30\epsilon/\sigma_{\text{LJ}}^2$ and $r_0 = 1.5\sigma_{\text{LJ}}$.

The simulations were conducted using the LAMMPS simulator [36], that solves Newton's equations of motion using a velocity-Verlet algorithm. The temperature T was maintained by presence of the Langevin dumping term with the coefficient $\zeta = 0.5\, m\tau^{-1}$, where $\tau = \sqrt{m\sigma_{\text{LJ}}^2/\epsilon}$ is the LJ time unit. The simulations were carried out in the cubic box with periodic boundary conditions in all three dimensions with equations of motion solved with the integration step $\Delta t = 0.005\tau$.

The initial conformations for the dumbbell polymers were generated using a self-avoiding walk technique generated by applying $20(2 + l)N$ symmetry operations on the simple cubic lattice [37] (see details on the pivot algorithm). This approach allowed us to start from a more compact conformation and save computation time since the method allows for more radical changes to the trajectories per step than the MD simulation. Note that the advantage of MD simulations is better sampling of conformations when calculating size ratios [38].

The simulations were run for up to 27 molecules in the simulation box, with the steric interactions between the molecules turned off to describe dilute solution conditions. The data for the averaging of observables were accumulated for a time period of at least three relaxation times of the corresponding systems.

We considered dumbbell polymers with degree of polymerization of rings $N = 50, 100, 150, 200, 250$, and 300 beads and degree of polymerization of linear backbones of $N_c = N/4, N/2, N, 3N/2$, and $2N$. For each of value of N_c we calculated universal size ratios g in the asymptotic limit, i.e., by removing the finite size effects via a least-squares fitting of the form $\tilde{g}_c(N) = g_c + C/N^{\Delta}$ where g_c and C are fitting constants and exponent Δ is defined below. In the calculation of the g factor [see Eq. (1)] we used the radius of gyration R_{linear}^2 of the corresponding linear chain of the same overall degree of polymerization as the dumbbell molecule. The values of R_{linear}^2 were derived from a fitting function, $R_{\text{linear}}^2 = aN^{2\nu}(1 + bN^{-\Delta})$, utilizing simulation data within the range of 100 to 600 beads. This range was selected to capture the anticipated scaling regime. For the fitting procedure the best known numeric values for the scaling exponent $\nu = 0.587\,597(7)$ and the correction to scaling exponent $\Delta = 0.528(12)$ were taken into account [39]. This allowed us to utilize the most accurate values of R_{linear}^2 in the calculation of the size ratio g_c. The fitting results yielded Person's coefficients ranging from 0.8 to 1 for the majority of data sets. However, there are two exceptions where the coefficient approaches 0.5, specifically for the ratio g_c with $l = 0.25$ and 0.5. These lower coefficients

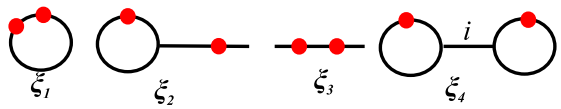

FIG. 2. Schematic representation of diagrams for use in calculation of the radius of gyration in the Gaussian approximation. The polymer is depicted by solid lines and the bullets represent the so-called restriction points s_1 and s_2.

can potentially be attributed to an increase in stiffness of the linear backbone. This is likely due to the backbone being relatively shorter compared to the ring segments in order to maintain the correct scaling behavior, resulting in a weaker quality of fit.

C. Wei's method

A macromolecule with complex architecture can be represented as a mathematical graph (network) where monomers are represented as vertices and chemical bonds between them are represented as bonds of the graph. A degree of a node corresponds to the monomer functionality. The size and shape characteristics for any polymer network can be calculated using Wei's method [24], which uses the Kirchhoff matrix and its eigenvalues.

A polymer that consists of N monomers is described by the Kirchhoff $N \times N$ matrix $\mathbf{K}$. All diagonal elements of this matrix K_{ii} are equal to degree of vertex i. The nondiagonal elements K_{ij} are equal to either -1 or 0 for i and j being connected or not connected, correspondingly. A Kirchhoff matrix of size $N \times N$ has $N-1$ nonzero eigenvalues $\lambda_2, \ldots, \lambda_M$:

$$\mathbf{K}\mathbf{Q}_i = \lambda_i \mathbf{Q}_i, \quad i = 1 \ldots M \tag{14}$$

and λ_1 is always zero. The size and shape characteristics within this model are given as functions of the above mentioned eigenvalues, thus the universal size ratio of Eq. (1) is defined as

$$g = \frac{\sum_{j=2}^{M} 1/\lambda_j^{\mathrm{DB}}}{\sum_{j=2}^{M} 1/\lambda_j^{\mathrm{linear}}}, \tag{15}$$

where λ_j^{DB} and $\lambda_j^{\mathrm{linear}}$ are the corresponding eigenvalues for the Kirchhoff matrix describing architecture of either a dumbbell or a linear chain.

The asphericity is given by the expression [24,40]

$$\langle A_d \rangle = \frac{d(d+2)}{2} \int_0^\infty dy \sum_{j=2}^{M} \frac{y^3}{(\lambda_j + y^2)^2} \left[\prod_{k=2}^{M} \frac{\lambda_k}{\lambda_k + y^2} \right]^{d/2}. \tag{16}$$

For a dumbbell architecture there are $N = (2+l)n + 2$ vertices with n being the number of vertices between the branching points (see Fig. 1) and every vertex having a degree $k > 1$.

III. RESULTS AND DISCUSSION

A. The radius of gyration of a dumbbell polymer and the universal size ratio

In the continuous chain model the radius of gyration of a dumbbell polymer is defined as

$$\langle R_g^2 \rangle = \frac{1}{2((2+l)L)^2} \sum_{i,j=0}^{2} \int_0^{L_i} \int_0^{L_j} \langle [\vec{r}_i(s_2) - \vec{r}_j(s_1)]^2 \rangle ds_1\, ds_2. \tag{17}$$

The actual calculation R_g^2 is performed by utilizing the following identity:

$$\langle [\vec{r}_i(s_2) - \vec{r}_j(s_1)]^2 \rangle = -2 \frac{d}{d|\vec{k}|^2} \xi(\vec{k})_{\vec{k}=0},$$
$$\xi(\vec{k}) \equiv \langle e^{-i\vec{k}(\vec{r}_i(s_2) - \vec{r}_j(s_1))} \rangle, \tag{18}$$

where the contributions to $\xi(\vec{k})$ are calculated using the diagrammatic technique. The schematic representations of the diagrams in the Gaussian approximation are displayed in Fig. 2. The first two diagrams are counted twice and the later two are counted only once. The final formula for the radius of gyration of a dumbbell polymer in the Gaussian approximation reads

$$\langle R_g^2 \rangle_0 = \frac{dL}{6}(l+1)(l^2+5l+3). \tag{19}$$

The corresponding universal size ratio [Eq. (1)] of a dumbbell polymer in the Gaussian approximation is given by the expression

$$g_c = \frac{(l+1)(l^2+5l+3)}{(l+2)^3}. \tag{20}$$

A significantly larger set of diagrams needs to be considered to estimate the radius of gyration of a dumbbell polymer with included excluded volume interactions. The calculation of R_g^2 in the first order of the perturbation theory gives the following expression:

$$\langle R_g^2 \rangle = \frac{3L^3(l+1)(l^2+5l+3)}{6} - u_0 R_1, \tag{21}$$

where the term R_1 accounting for steric interactions is given by

$$R_1 = \frac{288l^2 - 964l - 85}{72} \arcsin\left[(1+4l)^{-\frac{1}{2}}\right] - \frac{\pi(192l^2 - 332l + 47)}{72}$$
$$- \frac{1072l^6 + 8308l^5 + 862l^4 + 42588l^3 + 36505l^2 + 7630l + 420}{630\sqrt{l}(1+4l)(2l+1)} - \frac{\arctan[(2\sqrt{l})^{-1}]}{3}$$
$$- \frac{32l^4 - 1088l^3 - 2128l^2 - 1684l - 425}{144[(2l+1)\sqrt{4l+2}]} \left[\arctan\left(\frac{1+4l+\sqrt{4l+2}}{2\sqrt{l}} \right) - \arctan\left(\frac{1+4l-\sqrt{4l+2}}{2\sqrt{l}} \right) \right]. \tag{22}$$

From a number of previous studies it is known that ϵ expansion provides only a qualitative agreement with simulation and experimental data [7,41–44]. For this reason in this paper we do not provide the exact expression for g_c and limit our consideration to the Gaussian case [Eq. (20)] and the Douglas-Freed approximation. In the latter method the data were obtained numerically using the procedure described above.

In Fig. 3 we compare the results of our analytical calculations for the relative size g_c of ideal and real dumbbell polymers with respect to size of linear polymers and compare them with the results obtained from MD simulations. The data are plotted as a function of the relative degree of polymerization $l \equiv N_c/N$, i.e., the ratio between the number of monomers in a linear backbone and the number of monomers in a side ring. The red squares in the plot depict the data obtained using Wei's method, while the red dotted line represents the Gaussian approximation. These data sets correspond to an ideal dumbbell polymer and serve as the lower boundary for the value of g_c. The black dashed line represents the analytical results of the Douglas-Freed approximation for a real dumbbell polymer, i.e., with included excluded volume interactions. The plot displays the MD results using gray circles, representing the data for a finite system size of $N = 100$. Additionally, green circles indicate the data obtained from the correction to scaling analysis, i.e., for $N \to \infty$. We observe very good agreement between simulation data and the analytical predictions. The data obtained from all the methods consistently show that the size ratio for dumbbell architectures with $l \leqslant 2$ is $g_c < 1$ indicating a smaller molecular size of these polymers as compared to linear counterparts of the same molecular

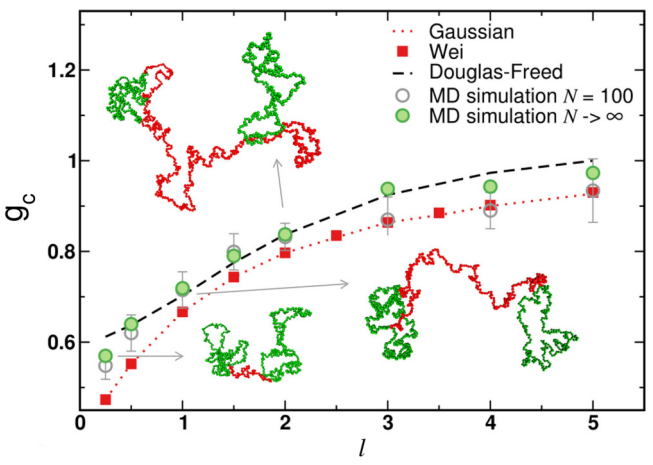

FIG. 3. Relative size ratio g_c of dumbbell-shaped polymers with respect to the size of the corresponding linear polymer with the same overall degree of polymerization. Data are plotted as a function of relative degree of polymerization l of linear chain monomers N_c to side ring monomers N. The lines represent theoretical prediction obtained for the Gaussian model (dotted line) and Douglas-Freed approximation (dashed line). Squares display the data obtained from Wei's method [see Eq. (15)]. Empty circles denote molecular dynamics results for fixed degree of polymerization $N = 100$ whereas full circles represent the values of g_c for infinitely long molecules ($N \to \infty$) obtained from correction to scaling analysis. The arrows indicate simulation snapshots for dumbbell polymers with given l.

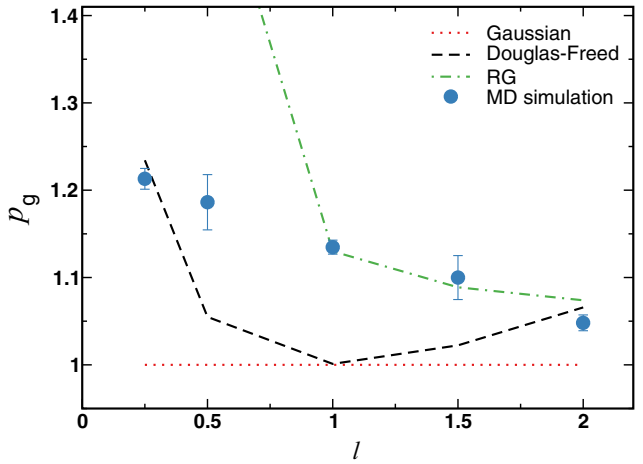

FIG. 4. Relative size ratio p_g of the backbone radius of gyration of dumbbell-shaped polymers to the radius of gyration of linear polymers plotted as a function of the relative degree of polymerization l. The lines represent theoretical predictions for the Gaussian conformations (dotted line), the Douglas-Freed approximation (dashed line), and the renormalization group calculations (dashed-dotted line). The symbols display the results of molecular dynamics simulations.

mass. The ratio g_c increases with increasing l. For Gaussian dumbbell conformations in the limit of $l \to \infty$ it leads to the value of $g_c = 1$ whereas for real dumbbell conformations the limiting value for g_c obtained from the Douglas-Freed approximation and MD simulations is observed for $l \approx 5$. These results corroborate the recent experimental study on dumbbell-shaped polymers carried out for large $l = 8$ where it was found that $g_c \approx 1$ [22]. Furthermore, it is noteworthy that when conducting analytical calculations for H polymers, which are macromolecular architectures with two linear side arms connected to each end of a linear backbone, the resulting value of g_c approaches 1 in the limit of $l \to \infty$. In particular, for H-shaped polymers with $l = 5$, the calculation yields $g_c = 0.95$ [45].

B. The radius of gyration of a dumbbell backbone and the corresponding size ratio

Another quantity that describes equilibrium conformation of a dumbbell molecule that is considered here is the gyration radius of a dumbbell backbone defined as

$$\langle r_g^2 \rangle_{\text{backbone}} = \frac{1}{2(lL)^2} \int_0^{L_c} \int_0^{L_c} \langle [\vec{r}0(s_2) - \vec{r}_0(s_1)]^2 \rangle. \quad (23)$$

The strategy of calculation is similar to that of the full radius of gyration. The general expression for $\langle r_g^2 \rangle_{\text{backbone}}$ is

$$\langle r_g^2 \rangle_{\text{backbone}} = \frac{dlL}{6}[1 - u_0 r_b(l, d) + \cdots], \quad (24)$$

where $r_b(l, d)$ is the contribution from the excluded volume interactions. The explicit formula for $\langle r_g^2 \rangle_{\text{backbone}}$ is provided in the Appendix [see Eq. (A12)]. To describe the influence of dumbbell side rings on the stretching of its backbone we introduce the relative size with respect to the linear chain of

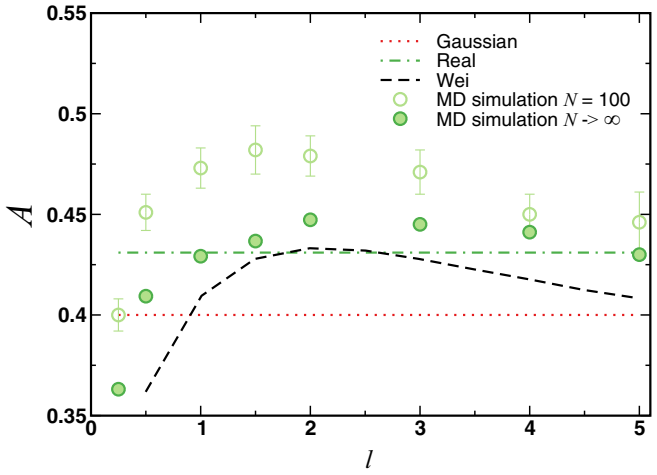

FIG. 5. Asphericity A of dumbbell-shaped polymers plotted as a function of the relative degree of polymerization l. The lines represent predictions for Gaussian conformations $A = 0.4$ [46] (dotted line) and real conformations $A = 0.431$ [47] (dashed-dotted line), i.e., with included steric interactions and the calculations using Wei's method [see Eq. (16)]. The symbols display the results of molecular dynamics simulations. Empty circles denote molecular dynamics results for fixed degree of polymerization $N = 100$ whereas full circles represent the values of A for infinitely long molecules ($N \to \infty$) obtained from correction to scaling analysis.

the same molecular weight as the backbone:

$$p_g = \frac{\langle r_g^2 \rangle_{\text{backbone}}}{\langle R_g^2 \rangle_{\text{linear}}}. \tag{25}$$

Unlike in the case of the universal size ratio g_c defined in Eq. (1), the quantity p_g does not depend on polymer topology for Gaussian conformations since it is simply equal to $p_g = 1$. In our analytical calculations of dumbbell conformations with steric interactions we accounted for topology-dependent contributions to p_g by considering the ϵ expansion and Douglas-Freed approximation. In Fig. 4 we plot the values of p_g as a function of l obtained from theoretical methods (lines) and MD simulations (symbols). For $l \geqslant 1$, the data calculated from ϵ-expansion method (dashed-dotted line) are in good agreement with the simulation results. However for $l \leqslant 1$ these results significantly overestimate MD data. The reason for this is the presence of logarithmic terms [$\propto \ln(l)$] in the ϵ expansion. Note that the results obtained from Douglas-Freed approximation (dashed line) do not provide a good agreement with the numerical results. This indicates necessity of the second-order perturbation calculations to correctly capture stretching of the backbone.

C. Asphericity

In what follows we focus on the analysis of a shape of dumbbell polymers using the asphericity factor. We emphasize that it is impossible to carry out path integration of the asphericity defined by Eq. (2) with the proper averaging. For this reason we limit our consideration to Wei's method, which provides good estimation of the asphericity for Gaussian conformations. Since in our calculations excluded volume interactions are introduced only as a small (perturbative) correction with respect to the Gaussian behavior, this approach is useful in predicting a qualitative behavior of the molecule's shape and includes molecular architecture of polymers. In Fig. 5 we display asphericity of ideal dumbbell molecules calculated from Wei's method and plot it as a function of l (dashed line). We observe that for $l \gg 1$ asphericity decays towards the limiting value of $A = 0.4$ [46] known for the Gaussian linear chain (dotted line). A similar trend is observed from our MD data (circles) but in this case the limiting value of asphericity for real dumbbell polymers is $A = 0.431$ (dashed-dotted line). The latter value of A is known from the previous studies on a linear chain in good solvent [47].

IV. CONCLUSIONS

In this paper we have studied the conformational properties of diluted dumbbell-shaped macromolecules consisting of two ring polymers connected to the ends of a linear spacer. For this purpose we used a combination of analytical calculations using field-theoretical methods and molecular dynamic

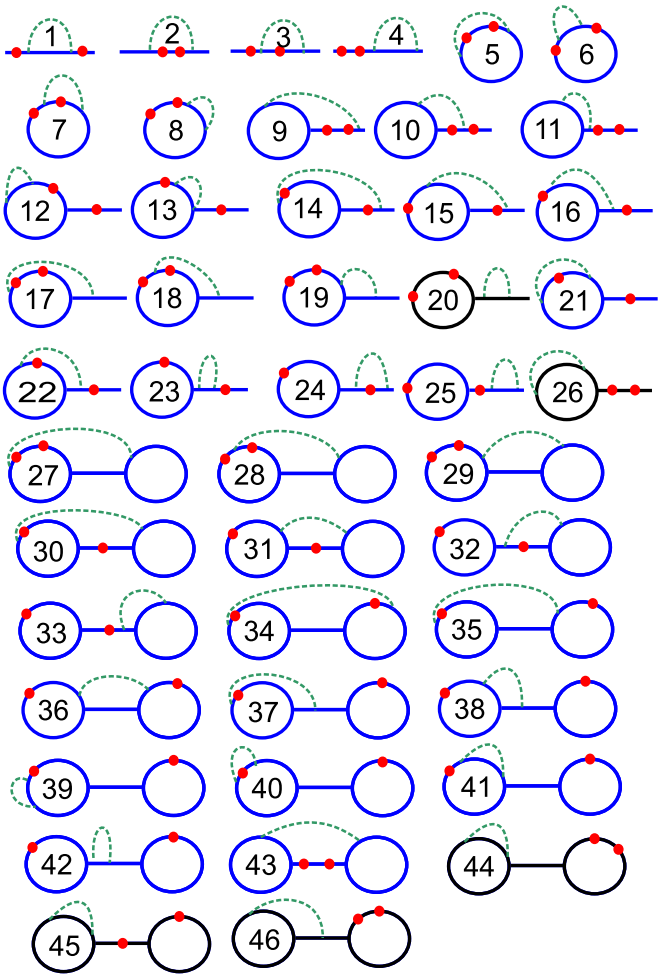

FIG. 6. Schematic representation of diagrams utilized in calculation of the radius of gyration radius in one loop approximation. The polymer is depicted by solid lines and the bullets represent the so-called restriction points s_1 and s_2. The dashed line represents the excluded volume interactions.

simulations. We have determined two relative size ratios g_c and p_g which are defined respectively as a ratio of the size R_g of a dumbbell and the size r_g of a linear spacer to the size R_{linear} of a linear chain of the same molecular weight. Our results indicate that conformations of dumbbells with short linear spacers are much more compact as compared to the linear polymer coils ($g_c < 0.65$). In this structural regime side rings have the major contribution to the global dumbbell conformation and cause stretching of the spacer segment ($p_g > 1$). Increasing the degree of polymerization of a spacer restores its conformational flexibility ($p_g \approx 1$) and gradually increases the size of a dumbbell molecule ($g_c \to 1$). Finally, for spacers that are much longer than side rings the size of a dumbbell matches the size of the corresponding linear chain ($g_c = 1$). The numerical data for g_c are in a very good agreement with the analytical predictions. Our theory accurately captures the conformational transition of dumbbells, shifting from configurations primarily governed by rings to configurations dominated by linear chains. This is evident in the observed increase of g_c as the length of the spacer grows. The results of this paper also corroborate the recent experiments that were carried out for dumbbells with long spacers which reported $g_c \approx 1$ [22].

ACKNOWLEDGMENTS

J.P. and K.H. would like to acknowledge support from the National Science Center, Poland (Grant No. 2018/30/E/ST3/00428) and the computational time at PL-Grid, Poland.

APPENDIX

Here we consider the details of the calculations of the contributions from the first order of perturbation theory to the partition function [Eq. (5)] and the corresponding calculations of the radius of gyration of a dumbbell polymer [Eq. (6)]. In both cases a certain set of diagrams has to be considered. For the partition function the diagrams are the same as for the Gaussian approximation of the gyration radius (see Fig. 2). The only difference is that we include interaction points instead of restriction points. The corresponding expressions are given below:

$$Z_1 = u(2\pi)^{-\frac{d}{2}}(2\pi L)^{-d}L^{2-\frac{d}{2}}\frac{\Gamma\left(1-\frac{d}{2}\right)^2(2-d)}{2\Gamma(3-d)}, \tag{A1}$$

$$Z_2 = u(2\pi)^{-\frac{d}{2}}(2\pi L)^{-d}L^{2-\frac{d}{2}}\left[\frac{2^{d-2}\sqrt{\pi}\Gamma\left(2-\frac{d}{2}\right)}{(2-d)\Gamma\left(\frac{5}{2}-\frac{d}{2}\right)} - \frac{2^{d-1}(4l+1)^{1-\frac{d}{2}}}{d-2}\text{hypergeom}\left(\frac{1}{2},\frac{d}{2}-1;\frac{3}{2};\frac{1}{4l+1}\right)\right], \tag{A2}$$

$$Z_3 = \frac{u(2\pi)^{-\frac{d}{2}}(2\pi L)^{-d}L_c^{2-\frac{d}{2}}}{\left(1-\frac{d}{2}\right)\left(2-\frac{d}{2}\right)}, \tag{A3}$$

$$Z_4 = u(2\pi)^{-\frac{d}{2}}(2\pi L)^{-d}L^{2-\frac{d}{2}}\int_{4l+1}^{4l+2}\frac{\left(\frac{x}{4}\right)^{-\frac{d}{2}}\text{hypergeom}\left(\frac{1}{2},\frac{d}{2};\frac{3}{2};\frac{1}{x}\right)}{2\sqrt{2-x+4l}}dx. \tag{A4}$$

Here we would like to point out the complications encountered in calculations of the term Z_4 which contains an integral. However, since this integral does not contain divergences in respect to $\epsilon = 4-d$, we can perform the expansion of the integrand. As in one loop approximation we have to consider only the terms with pole and terms $\propto \epsilon^0$. Note that we effectively calculate the expression Z_4 only for $d = 4$. Thus, the first-order contribution to the partition function will read

$$Z_1(l,d) = 2Z_1 + 2Z_2 + Z_3 + Z_4. \tag{A5}$$

The calculation for the radius of gyration is conducted in a similar manner and is also complicated. Here, we have to calculate the set of diagrams displayed in Fig. 6. Here, diagrams 25, 26, and 44–46 are reducible, as interaction points and restriction points do not share the same trajectory and thus the contributions are reduced to the product of the respective diagrams for the partition function and the Gaussian approximation for the radius of gyration. In general the calculation of the radius gyration is written as

$$\begin{aligned}\langle R_g^2\rangle &= Z^{-1}\left[\langle R_g^2\rangle_0 - u(\text{Sum of diagrams})\right] = \langle R_g^2\rangle_0 Z^{-1}\left(1-u\frac{(\text{Sum of diagrams})}{\langle R_g^2\rangle_0}\right)\\ &= \langle R_g^2\rangle_0(1+uZ_x)\left(1-u\frac{(\text{Sum of diagrams})}{\langle R_g^2\rangle_0}\right) = \langle R_g^2\rangle_0\left(1-u\left[\frac{(\text{Sum of diagrams})}{\langle R_g^2\rangle_0} - Z_x\right]\right).\end{aligned} \tag{A6}$$

Note that any contributions that appear in the product $Z_x\langle R_g^2\rangle_0$ cancel out. These are the diagrams mentioned above and some parts of the remaining diagrams, that in the case of the radius of gyration are easily identifiable. As an example we consider

diagrams 9–11:

$$\int_0^S ds \int_0^L dz \int_s^L ds_2 \int_s^{s_2} ds_1 \left(s_2 - s_1 - \frac{(s_2-s_1)^2}{s+z-\frac{s^2}{L}}\right)\left(s+z-\frac{s^2}{L}\right)^{-\frac{d}{2}}$$
$$+\int_0^S ds \int_0^L dz \int_s^L ds_2 \int_0^{s} ds_1 \left(s_2 - s_1 - \frac{(s-s_1)^2}{s+z-\frac{s^2}{L}}\right)\left(s+z-\frac{s^2}{L}\right)^{-\frac{d}{2}}$$
$$+\int_0^S ds \int_0^L dz \int_0^{s} ds_2 \int_0^{s_2} ds_1 (s_2-s_1)\left(s+z-\frac{s^2}{L}\right)^{-\frac{d}{2}}. \tag{A7}$$

Since all three integrals contain the same factor $(s+z)^{-\frac{d}{2}}$ that does not depend on the restriction points this expression can be rewritten as

$$\int_0^S ds \int_0^L dz \left[\int_0^{s} ds_2 \int_0^{s_2} ds_1 \left(s_2 - s_1 - \frac{(s_2-s_1)^2}{s+z-\frac{s^2}{L}}\right)\right.$$
$$\left.+\int_s^L ds_2 \int_0^{s} ds_1 \left(s_2 - s_1 - \frac{(s-s_1)^2}{s+z-\frac{s^2}{L}}\right)+\int_s^L ds_2 \int_s^{s_2} ds_1 (s_2-s_1)\right]\left(s+z-\frac{s^2}{L}\right)^{-\frac{d}{2}}. \tag{A8}$$

All the integrals inside the square brackets [...] contain the same term under the integration, that allows us to rewrite the expression as

$$\int_0^L ds \int_0^L dz \left[\int_0^{s} ds_2 \int_0^{s_2} ds_1 (s_2-s_1)+\int_s^L ds_2 \int_0^{s} ds_1 (s_2-s_1)+\int_s^L ds_2 \int_s^{s_2} ds_1 (s_2-s_1)\right]\left(s+z-\frac{s^2}{L}\right)^{-\frac{d}{2}}$$
$$+\int_0^S ds \int_0^L dz \left[\int_0^{s} ds_2 \int_0^{s_2} ds_1 \left(-\frac{(s_2-s_1)^2}{s+z-\frac{s^2}{L}}\right)+\int_s^L ds_2 \int_0^{s} ds_1 \left(-\frac{(s-s_1)^2}{s+z-\frac{s^2}{L}}\right)\right]\left(s+z-\frac{s^2}{L}\right)^{-\frac{d}{2}}. \tag{A9}$$

The last two terms in the first line can be joined since the limits of the integration over s_2 are the same and the integration over s_1 can be presented as one integral:

$$\int_0^S ds \int_0^L dz \left[\int_0^{s} ds_2 \int_0^{s_2} ds_1 (s_2-s_1)+\int_s^L ds_2 \int_0^{s_2} ds_1 (s_2-s_1)\right]\left(s+z-\frac{s^2}{L}\right)^{-\frac{d}{2}}$$
$$+\int_0^S ds \int_0^L dz \left[\int_0^{s} ds_2 \int_0^{s_2} ds_1 \left(-\frac{(s_2-s_1)^2}{s+z-\frac{s^2}{L}}\right)+\int_s^L ds_2 \int_0^{s} ds_1 \left(-\frac{(s-s_1)^2}{s+z-\frac{s^2}{L}}\right)\right]\left(s+z-\frac{s^2}{L}\right)^{-\frac{d}{2}}. \tag{A10}$$

The similar arguments now may be presented for the case of integration over s_2, so the final expression reads

$$\int_0^S ds \int_0^L dz \left(s+z-\frac{s^2}{L}\right)^{-\frac{d}{2}}\left[\int_0^L ds_2 \int_0^{s_2} ds_1 (s_2-s_1)\right]$$
$$+\int_0^S ds \int_0^L dz \left[\int_0^{s} ds_2 \int_0^{s_2} ds_1 \left(-\frac{(s_2-s_1)^2}{s+z-\frac{s^2}{L}}\right)+\int_s^L ds_2 \int_0^{s} ds_1 \left(-\frac{(s-s_1)^2}{s+z-\frac{s^2}{L}}\right)\right]\left(s+z-\frac{s^2}{L}\right)^{-\frac{d}{2}}. \tag{A11}$$

Here the first term is reducible. The more interesting part is that in the first order of the perturbation theory only the diagrams that correspond to excluded volume interactions between points on the same trajectory (diagrams 1–8, 12, 13, 20, 21, 23–26, 39–42, 44, and 45) contain poles in their ϵ expansions, that are not canceled by the partition sum. These diagrams are also easy to calculate. For the rest of the diagrams we perform calculations for either $d=4$ or 3 and take into account only the terms that are not canceled. This way it is easier to handle the analytical calculations. Note that an expression for the ϵ expansion will still in parts be calculated numerically. Results for $d=3$ are a bit more straightforward and thus are provided in the main part. As an example we present here the expressions for the radius of gyration of a dumbbell backbone for both $d=3$ and ϵ expansion:

$$\langle r_g^2\rangle_{\text{backbone}}(d=3) = \frac{3lL}{6}\left[1-u_0\left(-\frac{67}{315}-\frac{\pi(4l+1)}{24}+\frac{1}{12}(1/12)\arcsin\left[(4l+1)^{-\frac{1}{2}}\right](4l+1)\right.\right.$$
$$\left.\left.-\frac{\sqrt{l}(176l^4-128l^3-328l^2-130l-15)}{90(1+2l)(4l+1)}-\frac{2l^4}{9}\frac{\arctan\left(\frac{4l+1+\sqrt{2+4l}}{2\sqrt{l}}\right)-\arctan\left(\frac{4l+1-\sqrt{2+4l}}{2\sqrt{l}}\right)}{(1+2l)\sqrt{2+4l}}\right)\right], \tag{A12}$$

$$\langle r_g^2\rangle_{\text{backbone}}(d=4-\epsilon)=\frac{dlL}{6}\Bigg[1-u_0\Bigg(-\frac{2}{\epsilon}+\frac{13}{12}-\ln(l)+12l\int_0^1\frac{\operatorname{arctanh}\big((1-4z^2+4l+4z)^{-\frac{1}{2}}\big)}{(1-4z^2+4l+4z)^{\frac{5}{2}}}\,dz$$
$$-\frac{l\operatorname{arctanh}\big(2+4l)^{-\frac{1}{2}}\big)(8l+7)}{\sqrt{2+4l}(1+2l)}+\frac{4l\operatorname{arctanh}((4l+1)^{-\frac{1}{2}})(4l+3)}{(4l+1)^{\frac{3}{2}}}-\frac{(l-1)}{(1+2l)(4l+1)}$$
$$-\frac{2}{5}\frac{\ln(2)(10l+3)}{l^3}-\frac{1}{5}\frac{\ln(4l+1)(40l^2-22l-3)}{l^3(4l+1)}-\frac{1}{150}\frac{1650l^3+250l^2-614l-141)}{l^3(4l+1)}$$
$$-\frac{3}{16l^3}\int_0^1\frac{\ln\left(\frac{4l-x+1}{4l+1}\right)(-2(8l+3)(4l+1)^2+4(4l+1)(8l^2+12l+3)x-(112l^2+96l+18)x^2)}{\sqrt{x}(4l-x+1)^2}\,dx$$
$$-\frac{3}{16l^3}\int_0^1\frac{\ln\left(\frac{4l-x+1}{4l+1}\right)((32l+12)x^3-3x^4)}{\sqrt{x}(4l-x+1)^2}\,dx\Bigg)\Bigg]. \tag{A13}$$

[1] J. Roovers, Viscoelastic properties of polybutadiene rings, Macromolecules **21**, 1517 (1988).

[2] T. McLeish, Polymers without beginning or end, Science **297**, 2005 (2002).

[3] B. Duplantier, Statistical mechanics of polymer networks of any topology, J. Stat. Phys. **54**, 581 (1989).

[4] W. Fiers and R. L. Sinsheimer, The structure of the dna of bacteriophage ϕx174: III. Ultracentrifugal evidence for a ring structure, J. Mol. Biol. **5**, 424 (1962).

[5] H.-X. Zhou, Effect of catenation on protein folding stability, J. Am. Chem. Soc. **125**, 9280 (2003).

[6] B. H. Zimm and W. H. Stockmayer, The dimensions of chain molecules containing branches and rings, J. Chem. Phys. **17**, 1301 (1949).

[7] J. Douglas and K. F. Freed, Renormalization and the two-parameter theory, Macromolecules **17**, 2344 (1984).

[8] B. A. Laurent and S. M. Grayson, Synthetic approaches for the preparation of cyclic polymers, Chem. Soc. Rev. **38**, 2202 (2009).

[9] J. D. Halverson, W. B. Lee, G. S. Grest, A. Y. Grosberg, and K. Kremer, Molecular dynamics simulation study of nonconcatenated ring polymers in a melt. II. Dynamics, J. Chem. Phys. **134**, 204905 (2011).

[10] Y. Tezuka, Topological polymer chemistry for designing multicyclic macromolecular architectures, Polymer Journal **44**, 1159 (2012).

[11] Z. Jia and M. J. Monteiro, Cyclic polymers: Methods and strategies, J. Poly. Sci. A **50**, 2085 (2012).

[12] K. Zhang and G. N. Tew, Cyclic polymers as a building block for cyclic brush polymers and gels, Reactive and Functional Polymers **80**, 40 (2014)

[13] M. Kapnistos, M. Lang, D. Vlassopoulos, W. Pyckhout-Hintzen, D. Richter, D. Cho, T. Chang, and M. Rubinstein, Unexpected power-law stress relaxation of entangled ring polymers, Nat. Mater. **7**, 997 (2008).

[14] K. Zhang, M. A. Lackey, J. Cui, and G. N. Tew, Gels based on cyclic polymers, J. Am. Chem. Soc. **133**, 4140 (2011).

[15] Y. Doi, K. Matsubara, Y. Ohta, T. Nakano, D. Kawaguchi, Y. Takahashi, A. Takano, and Y. Matsushita, Melt rheology of ring polystyrenes with ultrahigh purity, Macromolecules **48**, 3140 (2015).

[16] A. Erbaş and J. Paturej, Friction between ring polymer brushes, Soft Matter **11**, 3139 (2015).

[17] J. E. Poelma, K. Ono, D. Miyajima, T. Aida, K. Satoh, and C. J. Hawker, Cyclic block copolymers for controlling feature sizes in block copolymer lithography, ACS Nano **6**, 10845 (2012).

[18] J. D. Halverson, G. S. Grest, A. Y. Grosberg, and K. Kremer, Rheology of Ring Polymer Melts: From Linear Contaminants to Ring-Linear Blends, Phys. Rev. Lett. **108**, 038301 (2012).

[19] Y. Doi, A. Takano, Y. Takahashi, and Y. Matsushita, Melt rheology of tadpole-shaped polystyrenes, Macromolecules **48**, 8667 (2015).

[20] Y. Doi, A. Takano, Y. Takahashi, and Y. Matsushita, Melt rheology of tadpole-shaped polystyrenes with different ring sizes, Soft Matter **16**, 8720 (2020).

[21] A. Rosa, J. Smrek, M. S. Turner, and D. Michieletto, Threading-induced dynamical transition in tadpole-shaped polymers, ACS Macro Letters **9**, 743 (2020).

[22] Y. Doi, A. Takano, Y. Takahashi, and Y. Matsushita, Viscoelastic properties of dumbbell-shaped polystyrenes in bulk and solution, Macromolecules **54**, 1366 (2021).

[23] J. A. Aronovitz and D. R. Nelson, Universal features of polymer shapes, J. Phys. (Paris) **47**, 1445 (1986).

[24] G. Wei, New approaches to shapes of arbitrary random walks, Physica A **222**, 155 (1995).

[25] S. F. Edwards, The statistical mechanics of polymers with excluded volume, Proc. Phys. Soc. London **85**, 613 (1965).

[26] L. Dai and P. S. Doyle, Trapping a knot into tight conformations by intra-chain repulsions, Polymers **9**, 57 (2017).

[27] L. Dai, C. B. Renner, and P. S. Doyle, Origin of Metastable Knots in Single Flexible Chains, Phys. Rev. Lett. **114**, 037801 (2015).

[28] D. Kivotides, S. Louise Wilkin, and T. G. Theofanous, Entangled chain dynamics of polymer knots in extensional flow, Phys. Rev. E **80**, 041808 (2009).

[29] M. L. Mansfield and J. F. Douglas, Properties of knotted ring polymers. II. Transport properties, J. Chem. Phys. **133**, 044904 (2010).

[30] Y. Kantor, Knots in polymers, Pramana **64**, 1011 (2005).

[31] E. Orlandini and S. G. Whittington, Statistical topology of closed curves: Some applications in polymer physics, Rev. Mod. Phys. **79**, 611 (2007).

[32] J. des Cloizeaux and G. Jannink, *Polymers in Solution: Their Modelling and Structure* (Clarendon, Oxford, 1991).

[33] Y. Oono, *Statistical Physics of Polymer Solutions: Conformation-Space Renormalization-Group Approach* (Wiley, New York, 1985), pp. 301–437.

[34] G. S. Grest, K. Kremer, and T. A. Witten, Structure of many arm star polymers: A molecular dynamics simulation, Macromolecules **20**, 1376 (1987).

[35] G. S. Grest and K. Kremer, Molecular dynamics simulation for polymers in the presence of a heat bath, Phys. Rev. A **33**, 3628 (1986).

[36] S. Plimpton, Fast parallel algorithms for short-range molecular dynamics, J. Comput. Phys. **117**, 1 (1995).

[37] N. Madras and A. D. Sokal, The pivot algorithm: A highly efficient monte carlo method for the self-avoiding walk, J. Stat. Phys. **50**, 109 (1988).

[38] K. Haydukivska, O. Kalyuzhnyi, V. Blavatska, and J. Ilnytskyi, Swelling of asymmetric pom-pom polymers in dilute solutions, Condens. Matter Phys. **25**, 23302 (2022).

[39] N. Clisby and B. Dünweg, High-precision estimate of the hydrodynamic radius for self-avoiding walks, Phys. Rev. E **94**, 052102 (2016).

[40] C. von Ferber, M. Bishop, T. Forzaglia, C. Reid, and G. Zajac, The shapes of simple three and four junction comb polymers, J. Chem. Phys. **142**, 024901 (2015).

[41] K. Haydukivska, O. Kalyuzhnyi, V. Blavatska, and J. Ilnytskyi, On the swelling properties of pom-pom polymers in dilute solutions. Part 1: Symmetric case, J. Mol. Liq. **328**, 115456 (2021).

[42] K. Haydukivska, V. Blavatska, J. S. Kłos, and J. Paturej, Conformational properties of hybrid star-shaped polymers comprised of linear and ring arms, Phys. Rev. E **105**, 034502 (2022).

[43] K. Haydukivska, V. Blavatska, and J. Paturej, Universal size ratios of gaussian polymers with complex architecture: Radius of gyration vs hydrodynamic radius, Sci. Rep. **10**, 14127 (2020).

[44] V. Blavatska and R. Metzler, Conformational properties of complex polymers: Rosette versus star-like structures, J. Phys. A **48**, 135001 (2015).

[45] K. Haydukivska and V. Blavatska, On the swelling properties of pom-pom polymers: impact of backbone length, Condens. Matter Phys. **26**, 1 (2023).

[46] G. Gaspari, R. Joseph, and A. Beldjenna, The shapes of open and closed random walks: A l/d expansion, J. Phys. A **20**, 3393 (1987).

[47] O. Jagodzinski, E. Eisenriegler, and K. Kremer, Universal shape properties of open and closed polymer chains: Renormalization group analysis and Monte Carlo experiments, J. Phys. I France **2**, 2243 (1992).